Enhancing light absorption in organic semiconductor thin films by one-dimensional gold nanowire gratings

Dominik A. Gollmer,[*] Christopher Lorch, Frank Schreiber, Dieter P. Kern, and Monika Fleischer[†]

Institute for Applied Physics and Center for Light-Matter-Interaction, Sensors and Analytics LISA+, Eberhard Karls Universität Tübingen,
Auf der Morgenstelle 10 and 15, 72076 Tübingen, Germany

The interaction of metallic plasmonic nanostructures and organic semiconductor thin films plays a crucial role in engineering light harvesting and energy transfer processes, e.g., for optoelectronic applications. Plasmonic resonances of the metal structures can be used to increase the light emission or absorption of organic molecules. Here small molecules are employed since they can form organic layers with a defined crystalline order and orientation of the transition dipole. Extinction measurements combined with numerical simulations of a hybrid system consisting of a gold nanowire grating and a thin film of diindenoperylene (DIP) are reported. The experimental results are compared to the simulations and indicate an enhanced absorption in the wavelength region corresponding to the transition from the highest occupied molecular orbital to the lowest unoccupied molecular orbital of DIP. This enhancement is found to be related to the localized field enhancement near the individual nanostructures as well as to grating-induced effects. Notably, the hybrid system also exhibits parallel lattice resonances, which have recently been discussed for two-dimensional (2D) gold nanostructure arrays. In this study a hybrid plasmonic-organic small molecule system exhibiting these modes is investigated. The results for this model system show a way to modify the optical properties of plasmonic nanostructures by collective effects to achieve stronger light-matter interaction in a wide range of hybrid plasmonic systems.

I. INTRODUCTION

Plasmonic nanostructures acting as optical antennas have been thoroughly investigated for different purposes in recent years. Due to their abilities to focus light to subwavelength volumes and to create strongly enhanced near fields near their surface, such nanostructures show high promise for applications, such as near-field optical microscopy and spectroscopy, biosensing, or light harvesting in optoelectronic devices [1–5]. Optical antennas can enhance the spontaneous emission or the light absorption of organic molecules in their vicinity, which has been related to their localized surface plasmon resonances (LSPRs) [6,7]. In chains or arrays of plasmonic nanostructures, collective grating-induced modes, sometimes called surface lattice resonances (SLRs), can occur in addition to the LSPRs of single particles [8–14]. These modes are related to so-called Rayleigh anomalies, which occur when light is diffracted by the grating into an angle of 90°, i.e., parallel to the surface [15,16]. The condition for the appearance of these anomalies is connected to the wave vector (k-vector) component of the light diffracted by the grating that is oriented perpendicular to the grating plane. If the grating is defined in the x-y plane, this vector is parallel to the z direction. The k-vector of the diffracted light can be written as [17,18]

$$\vec{k} = \{k_x, k_y, k_z\} = \left\{ k_{x0} + m_x \frac{2\pi}{p_x},\ k_{y0} + m_y \frac{2\pi}{p_y}, \right.$$
$$\left. \sqrt{n_i^2 k_0^2 - \left(k_{x0} + m_x \frac{2\pi}{p_x}\right)^2 - \left(k_{y0} + m_y \frac{2\pi}{p_y}\right)^2} \right\}, \quad (1)$$

with the initial incoming k-vector $\vec{k_0} = \{k_{x0}, k_{y0}, k_{z0}\}$ and its magnitude k_0, the grating orders m_x, $m_y = 0, \pm 1, \pm 2, \ldots$, and the period of the grating in x and y direction p_x, p_y. With this notation grating anomalies occur if $k_z = 0$, i.e., there is no propagation of the diffracted light normal to the plane of the grating [17]. For asymmetric configurations with different refractive indices n_i above and below the grating, this condition is fulfilled twice per grating order, once on the upper surface side ($n_i = n_1$) and once on the substrate side ($n_i = n_2$) [17].

So far little is known on coupling gratings to ordered films of small molecules. Compared to the more commonly investigated polymers, small molecules evaporated from the gas phase have the advantage that they can form crystalline films and have a preferred orientation relative to the substrate, and therefore a known orientation of the transition dipole moment. Different types of small molecules have been suggested as donor and acceptor materials for optoelectronic devices [19,20].

In previous studies, plasmonic gratings have been combined with organic dyes and semiconductors or dipolar emitters to experimentally and theoretically study the spontaneous emission in coupled hybrid systems [18,21]. The emission of dye molecules can be strongly enhanced and directed in such systems when they radiatively decay through the collective grating modes [18,21,22]. Furthermore, stimulated emission in such hybrid systems has been observed [23].

In addition to the enhancement of the emission, also the coupling of lattice resonances to molecules has been studied theoretically and experimentally [24,25]. However, in the studies of bare plasmonic chains and 2D gratings or of hybrid systems, mainly such lattice modes have been considered that occur when the electric field vector of the incident light is perpendicular to the plane defined by the wave vector of the incident light and the wave vector added through diffraction.

[*]dominik.gollmer@uni-tuebingen.de
[†]monika.fleischer@uni-tuebingen.de

These modes are strongly damped when the refractive indexes n_1 and n_2 differ [13,26]. Only recently also so-called parallel lattice modes, with the incident electric field vector parallel to this plane, were discussed for the case of 2D arrays [27,28]. In the former [27], also the occurrence of parallel lattice resonances in one-dimensional (1D) nanowire gratings is mentioned [17]. According to these studies [27,28] such parallel lattice resonances are much more robust (i.e., undergo less damping) under a refractive index mismatch of n_1 and n_2, which is unavoidable for structures located at surfaces. In addition, the enhanced near fields were shown to extend further away from the surface [27] such that they could interact with a larger volume of an organic layer on top. This different resonance configuration is therefore potentially advantageous for device applications. The far-field properties of 1D nanowire gratings were investigated in former studies [17,29]. In the latter spectrally sharp grating-induced effects in extinction spectra are visible.

In the present work we study the influence of grating-induced effects in 1D plasmonic gold nanowire gratings on the optical properties of a hybrid system consisting of the plasmonic system and an organic semiconductor thin film. For this purpose we fabricate flat 1D gold nanowire gratings for the investigation of far-field extinction spectra of gratings both without and with an organic thin film. The gratings offer the advantage that their plasmonic and lattice modes can be tailored via their geometrical parameters, and spectrally tuned by the width and the period of the lines. Correspondingly, the plasmonic grating can be engineered to match the optical properties of the organic semiconductor. The organic film consists of diindenoperylene (DIP) molecules. DIP is chosen because its structural and optical properties have been thoroughly studied, and its growth mechanisms are relatively well understood [30–32]. Also, DIP has already been successfully used in a study on plasmonic-organic interactions,

showing local signal enhancement by a plasmonic Au tip [33]. Additionally this material has been used in organic optoelectronic devices [19,34].

The results of the optical extinction measurements are complemented by numerical simulations and indicate that an enhanced absorption in the spectral region of the transition from the highest occupied molecular orbital (HOMO) to the lowest unoccupied molecular orbital (LUMO) of DIP can be induced by both the local field enhancement in the vicinity of the nanowires and the grating-induced modes. For suitable combinations of parameters, parallel lattice resonances can be observed in the hybrid 1D grating structures. With the use of collective parallel lattice resonances, additional degrees of freedom, i.e., the period or the illumination angle, are made available for tailoring the interactions in hybrid plasmonic-organic systems. This flexibility is essential for improving light absorption in the organic layer, or balancing gain vs loss mechanisms within hybrid optoelectronic systems. The advantage of collective resonances is not limited to the hybrid system shown here, but can be beneficial for hybrid plasmonic systems such as plasmonic/photovoltaic devices [35], for light-induced chemical reactions [36], or plasmonic sensor applications [37]. The coupling of organic-inorganic (or metallic) hybrid systems is not only relevant for direct optical effects, but also in the context of transport through organics via metallic contacts [38].

II. METHODS

A. Sample fabrication and extinction measurements

The gold nanowire gratings are fabricated on glass slides covered with an indium tin oxide (ITO) film of $\sim$50 nm thickness using conventional electron beam lithography and a lift-off process [Figs. 1(a)–1(d)] [39]. Polymethylmethacrylate (PMMA) positive resist is spin coated onto the glass/ITO
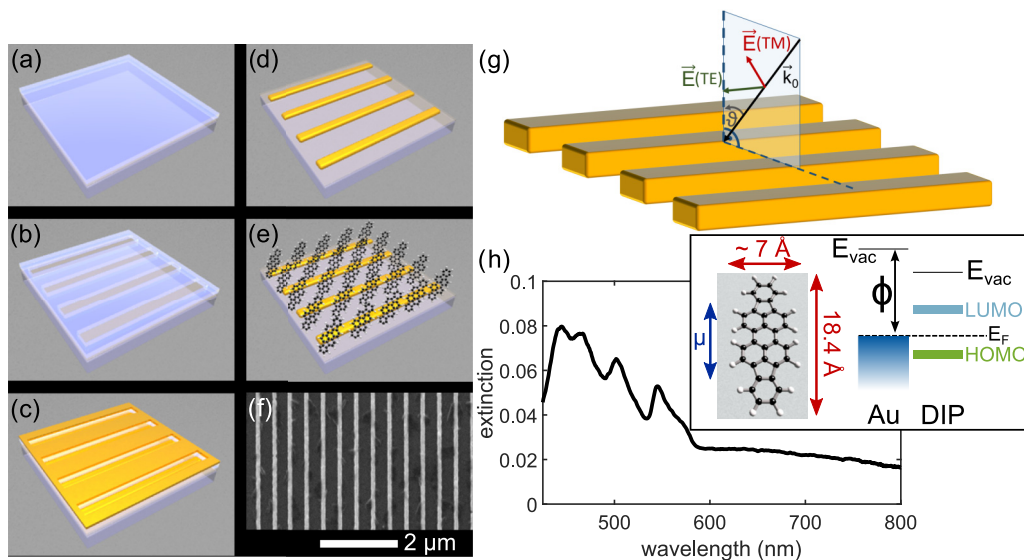
FIG. 1. Fabrication scheme of the nanowire grating: (a) substrate with PMMA positive resist, (b) electron beam lithography, (c) evaporation of gold, (d) lift-off, (e) evaporation of diindenoperylene, and (f) scanning electron microscope (SEM) image of the nanowire grating with a period of 394 nm and linewidth of 101 nm. (g) Illumination scheme for TM and TE polarization. (h) Extinction spectrum of 20 nm DIP on a glass/ITO substrate. The inset shows a model of the diindenoperylene molecule, with μ indicating the orientation of the transition dipole moment for the HOMO-LUMO-transition, and a schematic illustration of the energy levels of gold and DIP.

substrate. The resist is structured by an electron beam exposure (Philips XL 30) with subsequent development in a methyl isobutyl ketone (MIBK)/isopropanol solution, followed by thermal evaporation of 30 nm Au and lift-off in acetone. The mean period of the fabricated gratings used in this report is 394 ± 1 nm, and the mean width of the single nanowires is 101 ± 6 nm. The period and width of the wires were determined from at least ten measurements on different lines in a scanning electron microscope (SEM). A SEM image of the resulting grating is shown in Fig. 1(f). The DIP film with a thickness of $\sim$20 nm is deposited by organic molecular beam deposition ($T_{\text{substrate}} = 30\,^{\circ}$C) in an ultrahigh vacuum chamber [Fig. 1(e)] [40]. For investigating the optical properties of the grating and hybrid system the sample is illuminated in an inverted microscope (Nikon Eclipse Ti-U) by a white light beam (100 W halogen lamp) that is collimated to within $\pm 3^{\circ}$, while the transmitted light is detected through a $20\times$ objective. By inserting a pinhole of 200 µm diameter in the image plane of the microscope, light is spatially filtered [41]. Only light which passes the pinhole is detected by the spectrometer, such that specific areas of about 10 µm diameter on the sample can be optically analyzed. For investigating the polarization effects, a broadband linear polarizer is placed in the illumination light path, such that the grating can be illuminated by either transverse magnetic (TM) or transverse electric (TE) polarized light [Fig. 1(g)]. As a reference, the transmission spectrum of the halogen lamp through the glass/ITO substrate is used. The extinction spectra I_{ext} are calculated by $I_{\text{ext}} = (I_{\text{ref}} - I_{\text{trans}})/I_{\text{ref}}$, where I_{ref} is the transmission through glass/ITO and I_{trans} is the transmission at the position of the grating, the organic film without grating, or the hybrid system, respectively. In additional experiments the optical measurements were repeated on gratings with different widths on the same sample (not shown), for which similar results were obtained, only with shifts in the LSPR wavelengths.

In the extinction spectrum of the organic film [Fig. 1(h)], the typical absorption bands of DIP with its HOMO-LUMO transition band at $\sim$550 nm can be clearly observed [32]. An energy diagram for the gold/DIP hybrid system is schematically shown in the inset of Fig. 1(h). Note that for the absorption of DIP the orientation of the individual molecules with respect to the incoming light is crucially important since the dielectric tensor of DIP exhibits a strong anisotropy with its largest component along the molecule backbone [inset of Fig. 1(h)] [32]. For monolayers of organic semiconductors on metal substrates the molecules are typically found in a lying-down configuration [42–44]. Although there can still be reminiscences of this lying-down orientation also for thicker films on Au [45], the extinction spectra of the layers in the present study match the ones of films dominated by the standing-up configuration, with an average tilt angle of $\sim$17° relative to the substrate normal [32].

As expected, we find that the plasmon mode of the grating is strongly affected by the permittivity of the surrounding material [46]. To investigate and minimize the influence of the larger optical constant of DIP compared to air on the modes of the nanowire grating, we compare the results of the hybrid system (wire grating with organic thin film) with the same grating covered by aluminum oxide (film thickness 20 nm), which has a similar real part of the permittivity as DIP, but

a negligible imaginary part [32,47–49]. For this purpose, the organic film was removed in an oxygen plasma, followed by deposition of a 20 nm thick aluminum oxide film via electron beam evaporation.

B. Simulations

The simulations were performed using the finite elements method (COMSOL Multiphysics). The extinction spectra of the grating and the hybrid system as well as the absorption in the DIP film are calculated for transverse magnetic (TM) and transverse electric (TE) polarization of the incident light, i.e., the electric field vectors are oriented perpendicular (TM) or parallel (TE) to the nanowires [Fig. 1(g)]. The model consists of a 2D primitive cell with periodic boundary conditions. For the optical properties of Au [50], ITO [51], and DIP [32], data from the literature are used. Note that in many cases molecular systems exhibit highly anisotropic optical properties, which for a crystal are to be described with a (frequently low-symmetry) dielectric tensor [52]. For thin films, however, this often reduces to a uniaxial anisotropy [53,54]. For the permittivity of DIP, the anisotropy of DIP is taken into account, and the optical properties are included as a tensor. As a reference spectrum for the extinction curves, the transmission through a glass/ITO substrate is calculated. To take into account that the beam in the experiment is not perfectly collimated, the simulations are performed for different incident angles of 0° to 3°, varied in steps of 0.5° [ϑ in Fig. 1(g)]. The calculated spectra show the mean value of the extinction in this interval. The period of the grating and the wire width are taken from the experimentally determined mean values. For the wire height, the nominally evaporated gold film thickness is used.

For the determination of the spectrally resolved absorption enhancement in the organic thin film, the absorbed power in the organic thin film on the nanowires is calculated and then normalized by the absorbed power in an organic film of equal thickness without the gold nanowire grating. The mechanisms leading to the enhancement are investigated by comparing these simulations with simulations for a single nanowire. The dimensions of the nanowire are the same as for the nanowires in the grating. Additionally, for both systems, the grating and the single wire, the spectrally and spatially resolved distributions of the relative electric field strength along a line 15 nm above the substrate (respectively at half the height inside the nanowire) are calculated. For this purpose, the simulated electric field strengths 15 nm above substrates with nanowires are normalized to the field strengths at the same position, but simulated without nanowires.

III. RESULTS AND DISCUSSION

For the experimental studies a gold nanowire grating with a period of 394 nm, a width of 101 nm, and a height of 30 nm of the single wires was fabricated.

The grating was prepared on a glass substrate with a thin indium tin oxide layer (ITO, $\sim$50 nm, see Sec. II). The thickness of the DIP film is $\sim$20 nm, which is a typical thickness for pure DIP in organic thin film solar cells [19]. The DIP film is expected to be corrugated due to the underlying nanowires, nevertheless it should completely cover the grating structure [55]. The simulation model of the nanowire grating and the
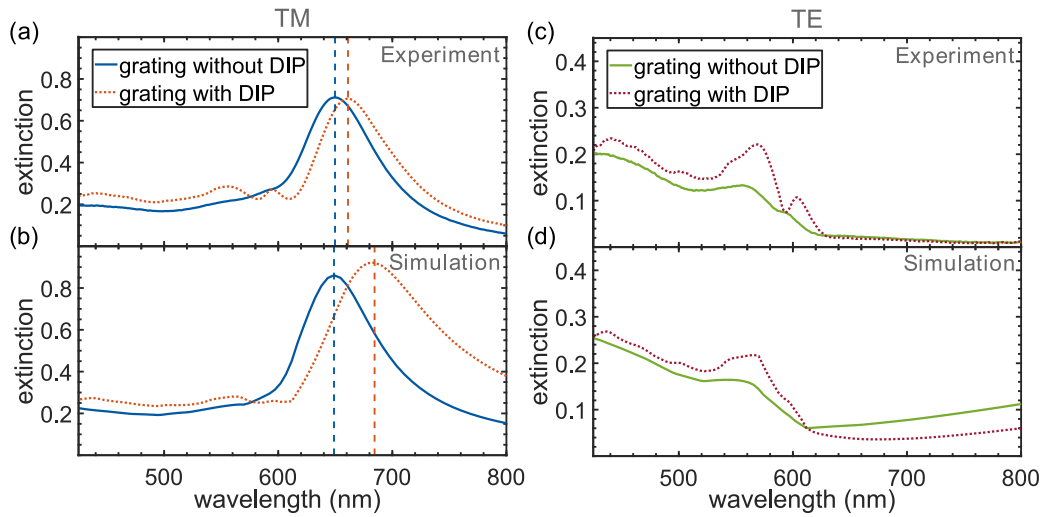
FIG. 2. Experimental [(a) and (c)] and simulated [(b) and (d)] extinction data of gold nanogratings for TM [(a) and (b)] and TE polarization [(c) and (d)]. The solid blue and green curves show the spectra without DIP, and the dotted orange and red curves the spectra of the hybrid system. The vertical dashed lines indicate the positions of the LSPRs.

hybrid system is designed according to the experimental properties (see Sec. II B). The fabrication scheme as well as a SEM image of the grating and the illumination geometry with the definition of TM and TE polarization are shown in Fig. 1 together with the optical properties of DIP.

The sample was now illuminated by white light polarized either parallel or perpendicular to the gold wires. Figure 2 shows the results of the extinction experiments [Figs. 2(a) and 2(c)] and the simulations [Figs. 2(b) and 2(d)] for TM polarized incident light [Figs. 2(a) and 2(b)] and for TE polarized light [Figs. 2(c) and 2(d)], respectively, each with a spectrum taken of the grating only and a spectrum taken with DIP on top of the grating (hybrid system). Here the extinction is shown, because when measuring transmission spectra, beside absorption also scattering contributes to the resulting spectra. Both effects are difficult to separate experimentally. Note that the absolute values of the extinction curves may be influenced by antireflection effects when adding the thin organic film.

Gratings with the same period but different widths of the wires show a similar optical response with a shift of the LSPR for different wire widths (not shown here). In the experiment the illumination was not perfectly collimated (opening angle light beam ∼3°), which is also considered in the simulations (see Sec. II B). The results of the simulations show comparable features as the experimental data. For TM polarization all spectra, experimental and simulated, exhibit a clear localized plasmon resonance at ∼650 nm for the nanowire grating, which is redshifted for the hybrid system due to the larger permittivity of the DIP film compared to air [46]. The shift in the experiment is smaller than expected from the simulations, maybe due to imperfect DIP coverage of the ridges in the experiment and the strong surface sensitivity of this mode. The LSPR stems from the excitation along the short axis of the nanowires. The experimental TM extinction spectrum of the hybrid system [Fig. 2(a)] depicts two additional maxima at ∼555 and ∼595 nm. These maxima are more prominent in the hybrid system than in the spectrum without DIP.

The simulated spectrum of the extinction of the bare grating for TM polarization fits very well to the experimental data [blue curves in Figs. 2(a) and 2(b)]. For the hybrid system the additional maxima at smaller wavelengths appear in the simulation as well, but are less pronounced compared to the experiment. Nevertheless, all features of the experimental data are reflected in the simulations.

For TE polarization the LSPRs vanish as expected [Figs. 2(c) and 2(d)], and modes at ∼570 and ∼605 nm are observed. For the spectrum of the hybrid system the modes appear much stronger than for the bare gratings. These modes seem to be grating induced and occur close to the wavelength of the Rayleigh anomaly, when the first grating order on the substrate side becomes evanescent [at about 591 nm for normal incidence according to Eq. (1)] [15,17,29,56]. The splitting of this grating-induced mode can be explained by the illumination of the sample with a not perfectly collimated beam (see Sec. II). This leads to the fact that for the first grating order the conditions of a grazing diffraction angle are fulfilled on the substrate side at two different wavelengths for each illumination angle [17]. When using Eq. (1) for calculating the two wavelengths of the Rayleigh anomalies on the substrate side for an illumination angle of 3°, the results (570 and 612 nm) are near the experimentally observed results for the extinction maxima (∼570 and ∼605 nm). Similar to the simulations for TM polarized incident light, the extinction in the simulation between ∼570 and ∼605 nm seems to be weaker than in the experiment. For longer wavelengths the simulation in Fig. 2(d) shows a rise of the extinction that does not appear in the experimental data. Simulations of the respective contributions of the absorption and reflection (not shown) indicate that the rise mostly results from reflection, which may be reduced in the experiment due to surface roughness. Since the optical properties of ITO depend on the exact preparation [57–60], also the optical data used for ITO in the simulations may deviate from the experimental
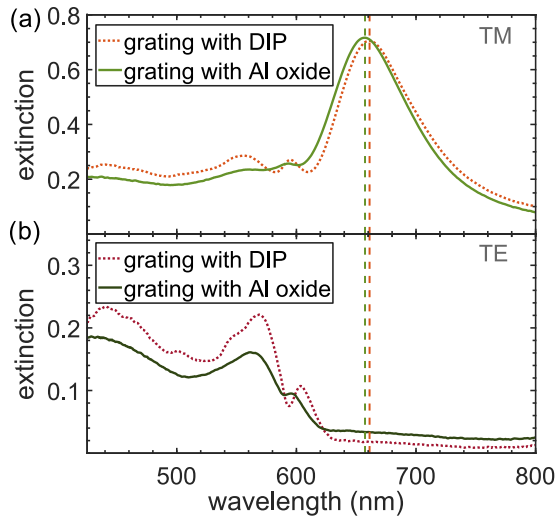
FIG. 3. Comparison of the extinction of gratings covered with DIP (dotted orange and red curves), as in Figs. 2(a) and 2(c) and with aluminum oxide (solid bright and dark green curves) for (a) TM and (b) TE polarization. The vertical dashed lines indicate that the LSPRs for the two hybrid systems in (a) are nearly identical.

FIG. 4. Simulated relative absorption of the DIP layer on a grating and a single wire, respectively, relative to DIP directly on a glass/ITO substrate for (a) TM and (b) TE polarization. Values larger than 1.0 correspond to absorption enhancement in the organic layer.

data in this range. However, this deviation only appears in the long-wavelength regime beyond the absorption bands of DIP.

Importantly, in the experimental data as well as in the simulations, for TM and TE polarization the extinction from 540 to 580 nm, near the HOMO-LUMO transition band, is increased for the hybrid system compared to the system without DIP. While an increase in the extinction from the added layer of DIP is to be expected, the magnitude of the increase surpasses the values of the pure DIP extinction as measured in Fig. 1(h). The results thus indicate an enhanced absorption due to collective effects in the nanowire grating. By the coupling between the corresponding local electric fields and the organic system, an interaction with the incoming light field beyond that of the pure organic system is achieved.

For further investigation of the origin of this enhanced extinction, the hybrid system is compared to the same grating covered with aluminum oxide (Fig. 3). Since the real part of the dielectric function of Al_2O_3 is comparable to that of DIP ($\sim$3.1–3.4) and the effect of the imaginary part can be neglected, permittivity-related effects are reduced [32,47–49]. In Fig. 3 the experimental extinction spectra of the hybrid organic system are compared to extinction spectra of the same grating, but covered with a 20 nm aluminum oxide layer. For TM polarization, the similar real parts of the permittivity of DIP and aluminum oxide can be recognized through the similar wavelength positions of the LSPR. In contrast to the extinction of the hybrid system with DIP, the extinction of the gratings covered with aluminum oxide is less strongly increased in the range of 540 to 580 nm, both for TM and TE polarization. Altogether, this indicates that an absorption effect beyond the pure sum of the absorptions in the DIP and the grating occurs in this wavelength region due to coupling and energy transfer between the different components of the hybrid system.

Experimentally, the quantitative determination of light absorbed in the DIP film or the grating, e.g., by differen-

tiating between scattered and absorbed light in extinction experiments, is a challenging issue. This is due to limitations of the numerical aperture of the objective as well as a dependence of the optical properties of the system on the exact illumination conditions, or antireflection effects in the layered system. Moreover, even with the knowledge of the absorption properties in the bare plasmonic or pure organic system, no quantitative conclusion on the absorption of the grating or the DIP film in the hybrid system is possible, since the reflection conditions within the system are modified by the hybrid system and the plasmonic properties are changed by the film. For this reason the influence of grating-induced effects on the light absorption in the organic material is investigated by further simulations, where the different contributions can be fully separated. Here only the absorption of light in the thin organic layer itself is considered, unlike in the simulations above (Fig. 2), where the extinction comprises scattering and absorption properties of the whole system. The absorption in the DIP film on the grating and on a single wire is normalized by the absorption of a 20 nm thick DIP film on glass/ITO substrate and plotted as a relative absorption in Fig. 4. Values above 1.0 thus show directly an absorption enhancement due to the presence of the plasmonic structures. Again the averaging over an interval of 0° to 3° is employed.

For TM polarization, besides the strong absorption enhancement at the plasmon resonance around 680 nm for the grating [Fig. 4(a)], a further maximum can be recognized around the position of the HOMO-LUMO transition near $\sim$555 nm. The relative absorption of a single nanowire for TM polarization shows similar features, only the enhancement at the plasmon resonance is weaker and the peak is broader. For TE polarization, the relative absorption for the grating system shows a maximum at the position of the grating anomaly around 590 nm [Fig. 4(b)]. For the single structure this
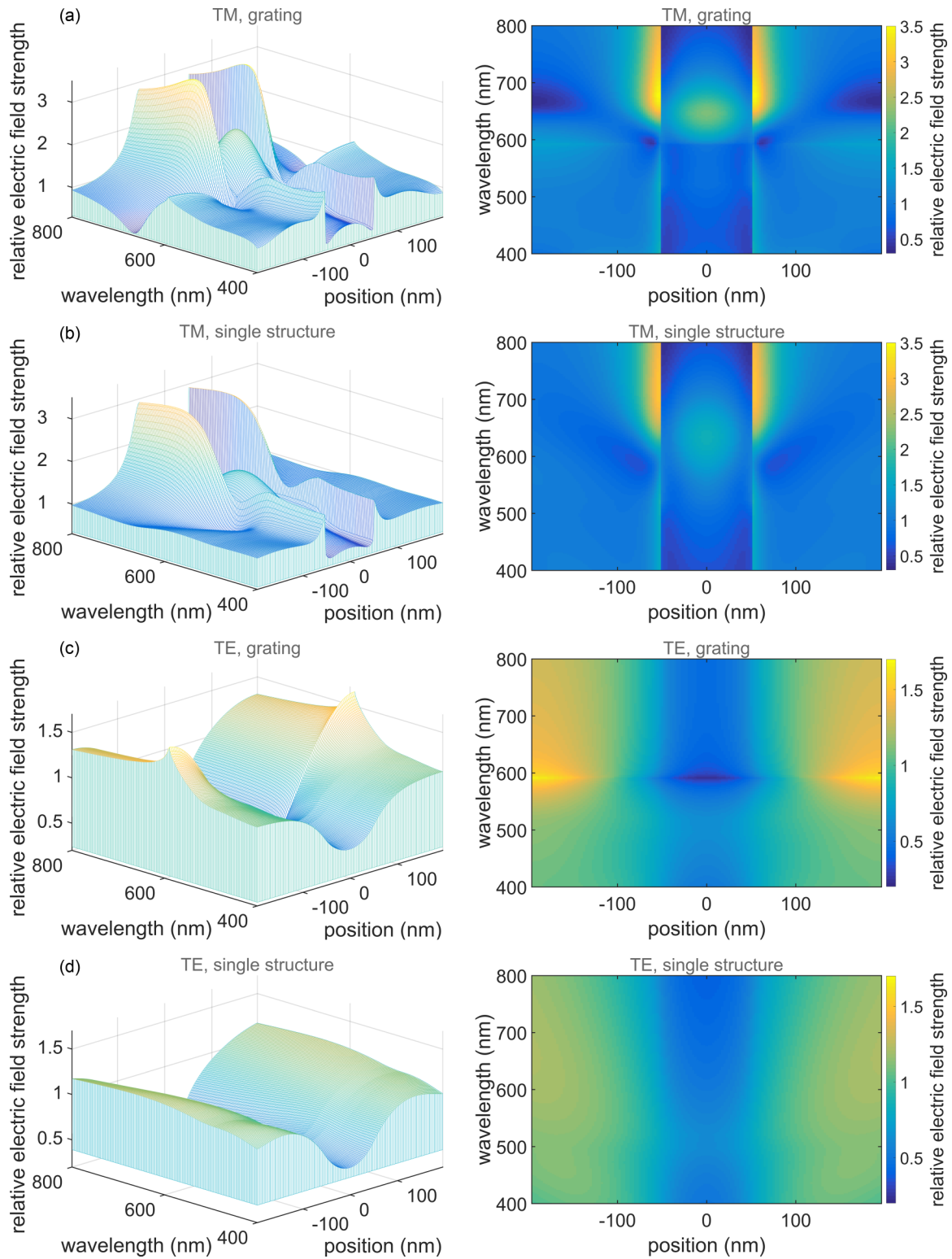
FIG. 5. Simulated distribution of the relative local electric field strength along a line 15 nm above the substrate (cross sectioning the wires at half their height) for excitation wavelengths of 400 to 800 nm. The distribution is shown for a unit cell, thus the nanowire center is positioned at 0 nm. The relative electric field strength is shown for a grating of nanowires (period = 394 nm) and a single wire with the same dimensions (width = 101 nm, height = 30 nm) for both TM and TE polarizations of the exciting field.

maximum vanishes. For wavelengths smaller than the grating anomaly the single structure shows a stronger enhancement, whereas for larger wavelengths the enhancement in the grating system is stronger.

The enhancement mechanisms for TM and TE polarization seem to have different physical origins. For TM polarization an enhancement around 555 nm can be observed for both the grating and the single structure, whereas for TE polarization
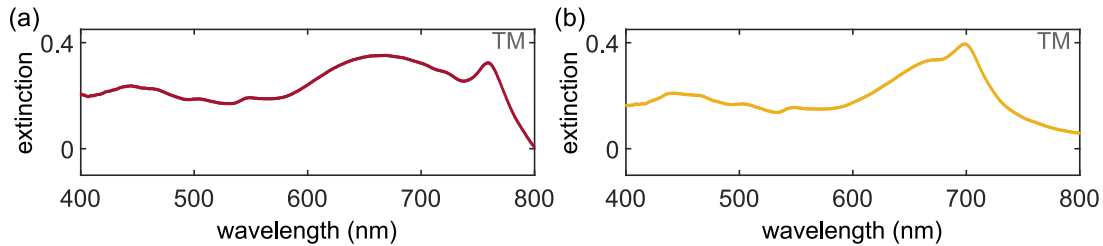
FIG. 6. Experimental extinction spectra of gold gratings with about (a) 500 nm and (b) 700 nm period and a 20 nm DIP film, measured with TM polarized illumination under perpendicular incidence. The parallel lattice modes (a) on the substrate side and (b) on the DIP/air side are clearly visible at about 750 and 700 nm.

a significant enhancement only exists for the grating. This observation suggests that the enhanced absorption in this wavelength region can be associated with plasmonic effects in the case of TM polarized excitation, and to grating effects for TE polarized excitation. According to this result, not only plasmon-induced near fields that are restricted to the positions of the metallic structures, but also collective grating-induced effects with fields that notably extend further into the organic layer can lead to an enhanced absorption in hybrid systems. This hypothesis is further tested in the following.

In Figs. 5(a)–5(d) the simulated distributions of the local electric field strength 15 nm above the substrate surface for a nanowire grating and a single nanowire (both without DIP layer) relative to the field strength at the same positions without nanowires are shown. The simulations are performed for normal incidence, both for TM and TE polarization, for wavelengths ranging from 400 to 800 nm. For TM polarization local near-field enhancement is observed close to the nanowire surface at the wavelength position of the LSPR. The electric field enhancement by the LSPR for the grating is stronger than for the single wire. This result agrees with the results for the absorption in the DIP layer in Fig. 4(a). The absorption enhancement at 555 nm may be attributed to the relative field maximum in this wavelength region, which can be recognized in the vicinity of the nanowire surface for the grating, but also for the single structure [Figs. 5(a) and 5(b)]. For TE polarization the relative field strength for the case of the grating [Fig. 5(c)] shows a sharp maximum just below 600 nm, which can be attributed to the grating anomaly.

The field enhancement is not localized at the nanostructure surface, but in between the nanowires. For any angles of incidence other than normal incidence two such maxima can be expected, with one maximum at a smaller and one maximum at a larger wavelength compared to normal incidence [17]. This field enhancement singularity can also be found for TM polarization at the same wavelength [Fig. 5(a)] because the effect of diffraction by the grating is polarization independent [cf. Eq. (1)] [17], only here it is less visible compared to the predominant plasmonic effects. For the single nanostructure no sharp features can be found for the relative electric field strength [Fig. 5(d)]. Therefore the absorption enhancement for TE polarization in the DIP on the grating below 600 nm seems indeed to be grating induced. Different angles of incidence can lead to a broadening of this absorption band [Fig. 4(b)].

For the hybrid gratings with 394 nm period that were discussed so far, the grating-induced mode due to the Rayleigh anomaly occurs at shorter wavelengths than the LSPR with hardly any spectral overlap. As an additional degree of freedom, the nanowire period can be tuned to shift the grating-induced mode across the spectrum. If for TM polarization this mode is matched to the LSPR or occurs at slightly higher wavelengths with sufficient spectral overlap, coupling between the modes is observed as a maximum in the extinction [17,27]. A parallel lattice mode is formed, since the electric field is oriented parallel to the direction of the grating coupling.

Figure 6 demonstrates that such parallel lattice modes were observed in hybrid gold nanowire-DIP gratings with about 500 nm period for the substrate-side grating mode at ∼760 nm [Rayleigh anomaly at 750 nm according to Eq. (1)], and with about 700 nm period for the DIP/air-side grating mode at ∼700 nm as expected from Eq. (1). These narrow band collective resonances offer another flexible handle for engineering the optical properties of hybrid systems.

In further experiments the influence of collective grating-induced modes near the HOMO-LUMO transition of DIP can be studied by changing the geometric parameters of the grating system [27,28]. As a first important outcome, this study shows that besides the near field connected with the LSPR, which is localized close to the grating lines, also parallel collective lattice resonances of a gold nanowire grating can be tailored to enhance the absorption of small-molecule organic thin films in a spectral range outside that of the localized plasmon mode. These collective resonances can be spectrally tuned via the grating geometry or the illumination angle and extend further into the organic film, creating a larger interaction volume.

IV. CONCLUSION

The optical properties of a gold nanowire grating coated with a thin organic film of diindenoperylene were investigated both experimentally and by simulations. The study aims at harnessing the plasmonic and lattice modes of the metallic grating to enhance the light absorption in the organic thin film of this hybrid system. Improving absorption over a broad spectral range is an important task for numerous light-harvesting applications. The optical characteristics of the nanowire grating can be tailored via the wire widths and spacings. Compared to previous studies on coupling gratings with organic layers, the choice of small molecules offers the advantages of well-defined thin films with a nanocrystalline order and known orientation of the transition dipoles. The localized surface plasmon resonance of the nanowires occurs at longer wavelengths compared to the HOMO-LUMO transition band of the DIP. The results of the extinction measurements of

the hybrid system are compared to measurements of the pure grating, and of a grating/aluminum oxide film system with a comparable real part of the dielectric function as the organic film. In excellent agreement with the simulations the results indicate an enhanced light absorption in the organic thin film over a broad spectral range upon interaction with the plasmonic grating. This enhanced absorption is a strong indication of coupling effects in the hybrid system beyond the pure sum of the absorptions of the constituents. The enhancement mechanism depends on the polarization of the incident electric field: for TM polarization the absorption enhancement seems to be associated with local field enhancement near the nanowire surfaces at smaller wavelengths than the spectral position of the LSPR. For TE polarization a grating-induced delocalized field enhancement appears to be the origin. For larger grating periods under TM polarization, the grating modes couple to the LSPR mode, and parallel lattice resonances are observed as a characteristic maximum in the extinction. These robust, narrow band and easily spectrally tunable parallel lattice resonances offer a new means for tailoring the absorption properties in hybrid systems, and for increasing the interaction volume of electric field enhancement within the organic layer.

[1] M. A. El-Sayed, Acc. Chem. Res. **34**, 257 (2001).

[2] P. Mühlschlegel, H. J. Eisler, O. J. F. Martin, B. Hecht, and D. W. Pohl, Science **308**, 1607 (2005).

[3] M. Fleischer, Nanotechnol. Rev. **1**, 313 (2012).

[4] C. Schäfer, D. A. Gollmer, A. Horrer, J. Fulmes, A. Weber-Bargioni, S. Cabrini, P. J. Schuck, D. P. Kern, and M. Fleischer, Nanoscale **5**, 7861 (2013).

[5] E. D. Fabrizio, S. Schlücker, J. Wenger, R. Regmi, H. Rigneault, G. Calafiore, M. West, S. Cabrini, M. Fleischer, N. F. van Hulst, M. F. Garcia-Parajo, A. Pucci, D. Cojoc, C. A. E. Hauser, and M. Ni, J. Opt. **18**, 063003 (2016).

[6] P. Anger, P. Bharadwaj, and L. Novotny, Phys. Rev. Lett. **96**, 113002 (2006).

[7] Y. Sugawara, T. A. Kelf, J. J. Baumberg, M. E. Abdelsalam, and P. N. Bartlett, Phys. Rev. Lett. **97**, 266808 (2006).

[8] M. Meier, A. Wokaun, and P. F. Liao, J. Opt. Soc. Am. B **2**, 931 (1985).

[9] V. A. Markel, J. Mod. Opt. **40**, 2281 (1993).

[10] S. Zou, N. Janel, and G. C. Schatz, J. Chem. Phys. **120**, 10871 (2004).

[11] N. Félidj, G. Laurent, J. Aubard, G. Lévi, A. Hohenau, J. R. Krenn, and F. R. Aussenegg, J. Chem. Phys. **123**, 221103 (2005).

[12] F. J. García de Abajo, Rev. Mod. Phys. **79**, 1267 (2007).

[13] B. Auguié and W. L. Barnes, Phys. Rev. Lett. **101**, 143902 (2008).

[14] V. G. Kravets, F. Schedin, and A. N. Grigorenko, Phys. Rev. Lett. **101**, 087403 (2008).

[15] R. Wood, London Edinburgh Dublin Philos. Mag. J. Sci. **4**, 396 (1902).

[16] L. Rayleigh, London Edinburgh Dublin Philos. Mag. J. Sci. **14**, 60 (1907).

[17] A. Christ, T. Zentgraf, J. Kuhl, S. G. Tikhodeev, N. A. Gippius, and H. Giessen, Phys. Rev. B **70**, 125113 (2004).

[18] G. Vecchi, V. Giannini, and J. Gómez Rivas, Phys. Rev. Lett. **102**, 146807 (2009).

[19] J. Wagner, M. Gruber, A. Hinderhofer, A. Wilke, B. Bröker, J. Frisch, P. Amsalem, A. Vollmer, A. Opitz, N. Koch, F. Schreiber, and W. Brütting, Adv. Funct. Mater. **20**, 4295 (2010).

[20] K. Broch, A. Aufderheide, L. Raimondo, A. Sassella, A. Gerlach, and F. Schreiber, J. Phys. Chem. C **117**, 13952 (2013).

[21] G. Pellegrini, G. Mattei, and P. Mazzoldi, J. Phys. Chem. C **115**, 24662 (2011).

[22] G. Lozano, D. J. Louwers, S. R. K. Rodriguez, S. Murai, O. T. A. Jansen, M. A. Verschuuren, and J. Gomez Rivas, Light Sci. Appl. **2**, e66 (2013).

[23] W. Zhou, M. Dridi, J. Y. Suh, C. H. Kim, D. T. Co, M. R. Wasielewski, G. C. Schatz, and T. W. Odom, Nat. Nano **8**, 506 (2013).

[24] S. R. K. Rodriguez, J. Feist, M. A. Verschuuren, F. J. Garcia Vidal, and J. Gómez Rivas, Phys. Rev. Lett. **111**, 166802 (2013).

[25] A. I. Väkeväinen, R. J. Moerland, H. T. Rekola, A. P. Eskelinen, J. P. Martikainen, D. H. Kim, and P. Törmä, Nano Lett. **14**, 1721 (2014).

[26] B. Auguié, X. M. Bendaña, W. L. Barnes, and F. J. García de Abajo, Phys. Rev. B **82**, 155447 (2010).

[27] A. Vitrey, L. Aigouy, P. Prieto, J. M. García-Martín, and M. U. González, Nano Lett. **14**, 2079 (2014).

[28] L. Lin and Y. Yi, Opt. Express **23**, 130 (2015).

[29] G. Schider, J. R. Krenn, W. Gotschy, B. Lamprecht, H. Ditlbacher, A. Leitner, and F. R. Aussenegg, J. Appl. Phys. **90**, 3825 (2001).

[30] A. C. Dürr, F. Schreiber, M. Münch, N. Karl, B. Krause, V. Kruppa, and H. Dosch, Appl. Phys. Lett. **81**, 2276 (2002).

[31] S. Kowarik, A. Gerlach, S. Sellner, F. Schreiber, L. Cavalcanti, and O. Konovalov, Phys. Rev. Lett. **96**, 125504 (2006).

[32] U. Heinemeyer, R. Scholz, L. Gisslén, M. I. Alonso, J. O. Ossó, M. Garriga, A. Hinderhofer, M. Kytka, S. Kowarik, A. Gerlach, and F. Schreiber, Phys. Rev. B **78**, 085210 (2008).

[33] D. Zhang, U. Heinemeyer, C. Stanciu, M. Sackrow, K. Braun, L. E. Hennemann, X. Wang, R. Scholz, F. Schreiber, and A. J. Meixner, Phys. Rev. Lett. **104**, 056601 (2010).

[34] U. Hörmann, J. Wagner, M. Gruber, A. Opitz, and W. Brütting, Phys. Status Solidi RRL **5**, 241 (2011).

[35] H. A. Atwater and A. Polman, Nat. Mater. **9**, 205 (2010).

[36] S. Linic, P. Christopher, and D. B. Ingram, Nat. Mater. **10**, 911 (2011).

[37] M. E. Stewart, C. R. Anderton, L. B. Thompson, J. Maria, S. K. Gray, J. A. Rogers, and R. G. Nuzzo, Chem. Rev. **108**, 494 (2008).

[38] F. Liscio, C. Albonetti, K. Broch, A. Shehu, S. D. Quiroga, L. Ferlauto, C. Frank, S. Kowarik, R. Nervo, A. Gerlach, S. Milita, F. Schreiber, and F. Biscarini, ACS Nano **7**, 1257 (2013).

[39] D. A. Gollmer, F. Walter, C. Lorch, J. Novák, R. Banerjee, J. Dieterle, G. Santoro, F. Schreiber, D. P. Kern, and M. Fleischer, Microelectron. Eng. **119**, 122 (2014).

[40] A. Hinderhofer and F. Schreiber, Chem. Phys. Chem. **13**, 628 (2012).

[41] P. Reichenbach, A. Horneber, D. A. Gollmer, A. Hille, J. Mihaljevic, C. Schäfer, D. P. Kern, A. J. Meixner, D. Zhang, M. Fleischer, and L. M. Eng, Opt. Express **22**, 15484 (2014).

[42] S. Duhm, S. Hosoumi, I. Salzmann, A. Gerlach, M. Oehzelt, B. Wedl, T.-L. Lee, F. Schreiber, N. Koch, N. Ueno, and S. Kera, Phys. Rev. B **81**, 045418 (2010).

[43] C. Bürker, N. Ferri, A. Tkatchenko, A. Gerlach, J. Niederhausen, T. Hosokai, S. Duhm, J. Zegenhagen, N. Koch, and F. Schreiber, Phys. Rev. B **87**, 165443 (2013).

[44] G. Heimel, S. Duhm, I. Salzmann, A. Gerlach, A. Strozecka, J. Niederhausen, C. Bürker, T. Hosokai, I. Fernandez Torrente, G. Schulze, S. Winkler, A. Wilke, R. Schlesinger, J. Frisch, B. Bröker, A. Vollmer, B. Detlefs, J. Pflaum, S. Kera, K. J. Franke, N. Ueno, J. I. Pascual, F. Schreiber, and N. Koch, Nat. Chem. **5**, 187 (2013).

[45] A. C. Dürr, N. Koch, M. Kelsch, A. Rühm, J. Ghijsen, R. L. Johnson, J. J. Pireaux, J. Schwartz, F. Schreiber, H. Dosch, and A. Kahn, Phys. Rev. B **68**, 115428 (2003).

[46] U. Kreibig and M. Vollmer, *Optical Properties of Metal Clusters* (Springer, Berlin, 1995).

[47] J. Cox, H. Hass, and J. Ramsey, J. Phys. **25**, 250 (1964).

[48] R. H. French, H. Müllejans, and D. J. Jones, J. Am. Ceram. Soc. **81**, 2549 (1998).

[49] Z. W. Zhao, B. K. Tay, S. P. Lau, and C. Y. Xiao, J. Vac. Sci. Technol. A **21**, 906 (2003).

[50] P. B. Johnson and R. W. Christy, Phys. Rev. B **6**, 4370 (1972).

[51] n&k Database, http://www.sspectra.com/sopra.html (Accessed 10 2016).

[52] M. I. Alonso, M. Garriga, N. Karl, J. O. Ossó, and F. Schreiber, Organ. Electron. **3**, 23 (2002).

[53] U. Heinemeyer, K. Broch, A. Hinderhofer, M. Kytka, R. Scholz, A. Gerlach, and F. Schreiber, Phys. Rev. Lett. **104**, 257401 (2010).

[54] M. I. Alonso, M. Garriga, J. O. Ossó, F. Schreiber, E. Barrena, and H. Dosch, J. Chem. Phys. **119**, 6335 (2003).

[55] R. Banerjee, J. Novák, C. Frank, M. Girleanu, O. Ersen, M. Brinkmann, F. Anger, C. Lorch, J. Dieterle, A. Gerlach, J. Drnec, S. Yu, and F. Schreiber, J. Chem. Phys. C **119**, 5225 (2015).

[56] L. Rayleigh, Proc. R. Soc. London. Ser. A **79**, 399 (1907).

[57] L.-j. Meng and M. P. dos Santos, Thin Solid Films **322**, 56 (1998).

[58] T. P. Nguyen, P. Le Rendu, N. N. Dinh, M. Fourmigué, and C. Mézière, Synth. Met. **138**, 229 (2003).

[59] Y. S. Jung, Thin Solid Films **467**, 36 (2004).

[60] X. Zhu, W. Sun, F. Tao, X. Cao, and X. Zhang, in *Proc. SPIE 8907, International Symposium on Photoelectronic Detection and Imaging 2013: Infrared Imaging and Applications*, 89072X (SPIE, Bellingham, WA, 2013).